Detection of atmospheric muon neutrinos with the IceCube 9-string detector

A. Achterberg,[31] M. Ackermann,[33] J. Adams,[11] J. Ahrens,[21] K. Andeen,[20] J. Auffenberg,[32] X. Bai,[23] B. Baret,[9] S. W. Barwick,[16] R. Bay,[5] K. Beattie,[7] T. Becka,[21] J. K. Becker,[13] K.-H. Becker,[32] M. Beimforde,[6] P. Berghaus,[8,15] D. Berley,[12] E. Bernardini,[33] D. Bertrand,[8] D. Z. Besson,[17] E. Blaufuss,[12] D. J. Boersma,[20] C. Bohm,[27] J. Bolmont,[33] S. Böser,[33] O. Botner,[30] A. Bouchta,[30] J. Braun,[20] C. Burgess,[27] T. Burgess,[27] T. Castermans,[22] D. Chirkin,[7] B. Christy,[12] J. Clem,[23] D. F. Cowen,[28,29] M. V. D'Agostino,[5] A. Davour,[30] C. T. Day,[7] C. De Clercq,[9] L. Demirörs,[23] F. Descamps,[14] P. Desiati,[20] T. DeYoung,[29] J. C. Diaz-Velez,[20] J. Dreyer,[13] J. P. Dumm,[20] M. R. Duvoort,[31] W. R. Edwards,[7] R. Ehrlich,[12] J. Eisch,[20] R. W. Ellsworth,[12] P. A. Evenson,[23] O. Fadiran,[3] A. R. Fazely,[4] K. Filimonov,[5] C. Finley,[20] M. M. Foerster,[29] B. D. Fox,[29] A. Franckowiak,[32] R. Franke,[33] T. K. Gaisser,[23] J. Gallagher,[19] R. Ganugapati,[20] H. Geenen,[32] L. Gerhardt,[16] A. Goldschmidt,[7] J. A. Goodman,[12] R. Gozzini,[21] T. Griesel,[21] S. Grullon,[20] A. Groß,[15] R. M. Gunasingha,[4] M. Gurtner,[32] C. Ha,[29] A. Hallgren,[30] F. Halzen,[20] K. Han,[11] K. Hanson,[20] D. Hardtke,[5] R. Hardtke,[26] J. E. Hart,[29] Y. Hasegawa,[10] T. Hauschildt,[23] D. Hays,[7] J. Heise,[31] K. Helbing,[32] M. Hellwig,[21] P. Herquet,[22] G. C. Hill,[20] J. Hodges,[20] K. D. Hoffman,[12] B. Hommez,[14] K. Hoshina,[20] D. Hubert,[9] B. Hughey,[20] J.-P. Hülß,[1] P. O. Hulth,[27] K. Hultqvist,[27] S. Hundertmark,[27] M. Inaba,[10] A. Ishihara,[10] J. Jacobsen,[7] G. S. Japaridze,[3] H. Johansson,[27] A. Jones,[7] J. M. Joseph,[7] K.-H. Kampert,[32] A. Kappes,[20,*] T. Karg,[32] A. Karle,[20] H. Kawai,[10] J. L. Kelley,[20] F. Kislat,[6] N. Kitamura,[20] S. R. Klein,[7] S. Klepser,[33] G. Kohnen,[22] H. Kolanoski,[6] L. Köpke,[21] M. Kowalski,[6] T. Kowarik,[21] M. Krasberg,[20] K. Kuehn,[16] M. Labare,[8] H. Landsman,[20] R. Lauer,[33] H. Leich,[33] D. Leier,[13] I. Liubarsky,[18] J. Lundberg,[30] J. Lünemann,[13] J. Madsen,[26] R. Maruyama,[20] K. Mase,[10] H. S. Matis,[7] T. McCauley,[7] C. P. McParland,[7] K. Meagher,[12] A. Meli,[13] T. Messarius,[13] P. Mészáros,[28,29] H. Miyamoto,[10] A. Mokhtarani,[7] T. Montaruli,[20,†] A. Morey,[5] R. Morse,[20] S. M. Movit,[28] K. Münich,[13] R. Nahnhauer,[33] J. W. Nam,[16] P. Nießen,[23] D. R. Nygren,[7] A. Olivas,[12] S. Patton,[7] C. Peña-Garay,[25] C. Pérez de los Heros,[30] A. Piegsa,[21] D. Pieloth,[33] A. C. Pohl,[30,‡] R. Porrata,[5] J. Pretz,[12] P. B. Price,[5] G. T. Przybylski,[7] K. Rawlins,[2] S. Razzaque,[28,29] P. Redl,[12] E. Resconi,[15] W. Rhode,[13] M. Ribordy,[22] A. Rizzo,[9] S. Robbins,[32] P. Roth,[12] F. Rothmaier,[21] C. Rott,[29] D. Rutledge,[29] D. Ryckbosch,[14] H.-G. Sander,[21] S. Sarkar,[24] K. Satalecka,[33] S. Schlenstedt,[33] T. Schmidt,[12] D. Schneider,[20] D. Seckel,[23] B. Semburg,[32] S. H. Seo,[29] Y. Sestayo,[15] S. Seunarine,[11] A. Silvestri,[16] A. J. Smith,[12] C. Song,[20] J. E. Sopher,[7] G. M. Spiczak,[26] C. Spiering,[33] M. Stamatikos,[20,§] T. Stanev,[23] T. Stezelberger,[7] R. G. Stokstad,[7] M. C. Stoufer,[7] S. Stoyanov,[23] E. A. Strahler,[20] T. Straszheim,[12] K.-H. Sulanke,[33] G. W. Sullivan,[12] T. J. Sumner,[18] I. Taboada,[5] O. Tarasova,[33] A. Tepe,[32] L. Thollander,[27] S. Tilav,[23] M. Tluczykont,[33] P. A. Toale,[29] D. Tosi,[33] D. Turčan,[12] N. van Eijndhoven,[31] J. Vandenbroucke,[5] A. Van Overloop,[14] G. de Vries-Uiterweerd,[31] V. Viscomi,[29] B. Voigt,[33] W. Wagner,[29] C. Walck,[27] H. Waldmann,[33] M. Walter,[33] Y.-R. Wang,[20] C. Wendt,[20] C. H. Wiebusch,[1] G. Wikström,[27] D. R. Williams,[29] R. Wischnewski,[33] H. Wissing,[1] K. Woschnagg,[5] X. W. Xu,[4] G. Yodh,[16] S. Yoshida,[10] and J. D. Zornoza[20,‖]

(IceCube Collaboration)

[1]*III Physikalisches Institut, RWTH Aachen University, D-52056 Aachen, Germany*
[2]*Department of Physics and Astronomy, University of Alaska Anchorage, 3211 Providence Dr., Anchorage, Alaska 99508, USA*
[3]*CTSPS, Clark-Atlanta University, Atlanta, Georgia 30314, USA*
[4]*Department of Physics, Southern University, Baton Rouge, Louisiana 70813, USA*
[5]*Department of Physics, University of California, Berkeley, California 94720, USA*
[6]*Institut für Physik, Humboldt-Universität zu Berlin, D-12489 Berlin, Germany*
[7]*Lawrence Berkeley National Laboratory, Berkeley, California 94720, USA*
[8]*Université Libre de Bruxelles, Science Faculty CP230, B-1050 Brussels, Belgium*
[9]*Vrije Universiteit Brussel, Dienst ELEM, B-1050 Brussels, Belgium*
[10]*Department of Physics, Chiba University, Chiba 263-8522 Japan*
[11]*Department of Physics and Astronomy, University of Canterbury, Private Bag 4800, Christchurch, New Zealand*
[12]*Department of Physics, University of Maryland, College Park, Maryland 20742, USA*
[13]*Department of Physics, Universität Dortmund, D-44221 Dortmund, Germany*
[14]*Department of Subatomic and Radiation Physics, University of Gent, B-9000 Gent, Belgium*
[15]*Max-Planck-Institut für Kernphysik, D-69177 Heidelberg, Germany*
[16]*Department of Physics and Astronomy, University of California, Irvine, California 92697, USA*
[17]*Department of Physics and Astronomy, University of Kansas, Lawrence, Kansas 66045, USA*
[18]*Blackett Laboratory, Imperial College, London SW7 2BW, United Kingdom*
[19]*Department of Astronomy, University of Wisconsin, Madison, Wisconsin 53706, USA*

[20]Department of Physics, University of Wisconsin, Madison, Wisconsin 53706, USA
[21]Institute of Physics, University of Mainz, Staudinger Weg 7, D-55099 Mainz, Germany
[22]University of Mons-Hainaut, 7000 Mons, Belgium
[23]Bartol Research Institute and Department of Physics and Astronomy, University of Delaware, Newark, Delaware 19716, USA
[24]Department of Physics, University of Oxford, 1 Keble Road, Oxford OX1 3NP, United Kingdom
[25]Institute for Advanced Study, Princeton, New Jersey 08540, USA
[26]Department of Physics, University of Wisconsin, River Falls, Wisconsin 54022, USA
[27]Department of Physics, Stockholm University, SE-10691 Stockholm, Sweden
[28]Department of Astronomy and Astrophysics, Pennsylvania State University, University Park, Pennsylvania 16802, USA
[29]Department of Physics, Pennsylvania State University, University Park, Pennsylvania 16802, USA
[30]Division of High Energy Physics, Uppsala University, S-75121 Uppsala, Sweden
[31]Department of Physics and Astronomy, Utrecht University/SRON, NL-3584 CC Utrecht, The Netherlands
[32]Department of Physics, University of Wuppertal, D-42119 Wuppertal, Germany
[33]DESY, D-15735 Zeuthen, Germany

(Received 12 May 2007; published 19 July 2007)

The IceCube neutrino detector is a cubic kilometer TeV to PeV neutrino detector under construction at the geographic South Pole. The dominant population of neutrinos detected in IceCube is due to meson decay in cosmic-ray air showers. These atmospheric neutrinos are relatively well understood and serve as a calibration and verification tool for the new detector. In 2006, the detector was approximately 10% completed, and we report on data acquired from the detector in this configuration. We observe an atmospheric neutrino signal consistent with expectations, demonstrating that the IceCube detector is capable of identifying neutrino events. In the first 137.4 days of live time, 234 neutrino candidates were selected with an expectation of $211 \pm 76.1(\text{syst}) \pm 14.5(\text{stat})$ events from atmospheric neutrinos.

DOI: 10.1103/PhysRevD.76.027101 PACS numbers: 95.55.Vj, 95.85.Ry, 96.50.sf

I. THE ICECUBE DETECTOR

The IceCube neutrino detector is being deployed in the deep ice below the geographic South Pole [1]. When completed, the detector will consist of two components. The InIce detector is a cubic kilometer of instrumented ice between 1.5 and 2.5 kilometers below the surface. A cubic kilometer has been long noted as the required scale to detect astrophysical neutrino sources above the atmospheric neutrino background (see, e.g. [2–4]). The IceTop detector is a square-kilometer air-shower array at the surface. This analysis concerns data from the InIce detector exclusively.

The InIce detector consists of an array of light-sensitive digital optical modules (DOMs) [5], deployed 17 meters apart in strings of 60. Strings are arranged on a hexagonal grid with a spacing of 125 meters. The DOMs house a 10-inch photomultiplier tube (PMT) and electronics to acquire, digitize, and time stamp pulse waveforms from the PMT. With a waveform fit for fine timing, the timing resolution for individual photon arrivals is expected to be less than 2 nanoseconds [5]. In 2006, the DOMs were operated in local coincidence (LC) with their neighbors, meaning that a triggered DOM's waveform was only transmitted to the surface if an adjacent DOM on the string also triggered within ± 1000 ns. The surface data acquisition system forms triggered detector-wide events if 8 or more DOMs are read out in 5 μs.

The detector is being deployed in stages during austral summers from 2004 to 2011. After the 2005–2006 season, the InIce detector consisted of 9 strings, termed IC-9.

IceCube is optimized for the detection of muon neutrinos in the TeV to PeV energy range. It is sensitive to these muon neutrinos (and muon antineutrinos) by detecting Cherenkov light from the secondary muon produced when the neutrino interacts in or near the instrumented volume. Neutrino-induced muons are separated from air-shower-induced muons by looking only for muons moving upward through the detector. Up-going muon events must be the product of a neutrino interaction near the detector, since neutrinos are the only known particles that can traverse the Earth without interacting.

II. ATMOSPHERIC NEUTRINOS

Neutrinos produced in cosmic-ray air showers at the Earth are known as atmospheric neutrinos and form the chief background to potential astrophysical neutrino observation. The atmospheric neutrino spectrum is relatively well understood [6,7] and has been measured up to 10^5 GeV by AMANDA [8]. Atmospheric neutrinos from the decay of charmed mesons can contribute significantly above 10^4 GeV, depending on the model (see e.g. [9–11]).

*On leave of absence from Universität Erlangen-Nürnberg, Physikalisches Institut, D-91058, Erlangen, Germany
†On leave of absence from Università di Bari, Dipartimento di Fisica, I-70126, Bari, Italy
‡Affiliated with Department of Chemistry and Biomedical Sciences, Kalmar University, S-39182 Kalmar, Sweden
§NASA Goddard Space Flight Center, Greenbelt, MD 20771, USA
‖Affiliated with IFIC (CSIC-Universitat de València), A. C. 22085, 46071 Valencia, Spain

This prompt component is not well known due to uncertainties in the charmed meson production, but with the present exposure of IC-9, this prompt component is negligible and it is presently neglected.

III. RESULTS

Data acquired from the IC-9 detector in 2006 between June and November has been searched for up-going neutrino candidates. The search proceeds by a series of cut levels intended to remove down-going events as shown in Table I. Initially, hit cleaning is applied which removes all DOM hits which fall out of a 4 μs time window, and all DOM hits without another DOM hit within a radius of 100 meters and within a time of 500 ns. After hit cleaning, we retrigger, insisting that at least 8 DOM hits survive hit cleaning. Simple first-guess reconstruction algorithms running at the South Pole were used to filter out clearly down-going events. Events with fewer than 11 DOMs hit were also filtered to meet bandwidth constraints from the South Pole. The remaining events were transmitted to the data center in the northern hemisphere via satellite and constitute the filter level of the analysis. At the data center, we reconstructed the direction of events using a maximum-likelihood technique similar to the AMANDA muon reconstruction [12]. Events which were reconstructed as down-going were discarded. Despite the fact that remaining events appear up-going, the data is still dominated by misreconstructed down-going events. These down-going events are removed by additional quality cuts. Events which pass these quality cuts constitute the neutrino candidate data set.

Simulated events fall into the three categories shown in Table I. ''Single shower'' events arise from single cosmic-ray air showers in the atmosphere above IceCube and result in a single muon or bundle of collinear muons in IC-9. ''Double shower'' events come from two uncorrelated air showers which happen to occur within the 5 μs event window. The CORSIKA [13] air shower simulation program was used for the simulation of down-going single and double air shower events. Finally, ''atmospheric neutrino'' events are muon neutrino events from pion and kaon decay in air showers in the northern hemisphere. The atmospheric neutrino model of [14] and its extension up to TeV energies [15] as well as the cross section parametrization of [16] were used to model the up-going muon rates due to atmospheric neutrinos.

The events which are reconstructed as up-going are completely dominated by down-going muons from single and double-shower cosmic-ray events. Misreconstructed events are typically of low quality as measured by two parameters, the number of direct hits N_{dir}, and the direct length L_{dir}. A direct hit is a photon arrival in a DOM which is detected between -15 and $+75$ ns of the time expected from the reconstructed muon with no scattering. N_{dir} is the total number of direct hits in an event. The direct length L_{dir} represents the length of the reconstructed muon track along which direct hits are observed. An event with a large number of direct hits and a large direct length is a better quality event because the long lever arm of many unscattered photon arrivals increases confidence in the event reconstruction. The strength of the quality cuts can be represented by a dimensionless number S_{cut} which corresponds to cuts of $N_{\mathrm{dir}} \geq S_{\mathrm{cut}}$ and $L_{\mathrm{dir}} > 25 \cdot S_{\mathrm{cut}}$ meters. In addition to these quality cuts, we impose a cut requiring that events have no more than 46 DOMs hit, which eliminates only about 1% of the final event sample. The purpose of this cut is to leave the high-multiplicity data blinded for an anticipated search for a high-energy diffuse neutrino flux. Figure 1 shows how many events remain as we turn the cut strength up and increase the signal-to-noise ratio. The accurate simulation of misreconstructed down-going events requires excellent modeling of both the depth-dependent ice properties and DOM sensitivity. In this initial study we observe a 60%–80% rate discrepancy for misreconstructed events up to a cut level of about $S_{\mathrm{cut}} = 8$ or so. Nevertheless, over more than 4 orders of magnitude, the background simulation tracks the data, the number of wrongly reconstructed tracks is reduced, and for $S_{\mathrm{cut}} \geq 10$, the data behaves as expected for atmospheric neutrinos. From simulation, we expect neutrinos with energies be-

TABLE I. Event passing rates (Hz). Shown are the event passing rates through different processing levels for the simulated event categories and for experimental data. The trigger level comprises the events triggering the detector after hit cleaning and retriggering. The filter level comprises events which passed the online filtering conditions. Rates are also shown for events which reconstruct as up-going with and without the final quality cuts applied (see the text for cut definition). Note that the rates from air shower events have been multiplied by 0.90 so that the simulation and data agree at trigger level. This is consistent with an approximately 20% uncertainty in the absolute cosmic-ray flux. For the final sample, statistical errors are given for the data and systematic errors are given for the atmospheric neutrino simulation.

Criterion satisfied	Data	Single shower	Double shower	Atmospheric neutrinos
Trigger level	124.5	124.5	1.5	6.6×10^{-4}
Filter level	6.56	4.96	0.45	3.7×10^{-4}
Up-going ($S_{\mathrm{cut}} = 0$)	0.80	0.49	0.21	3.3×10^{-4}
Up-going ($S_{\mathrm{cut}} = 10$)	$1.97 \times 10^{-5} \pm 0.12 \times 10^{-5}$	—	—	$1.77 \times 10^{-5} \pm 0.63 \times 10^{-5}$
Up-going ($S_{\mathrm{cut}} = 10$ and $\theta > 120$)	$1.19 \times 10^{-5} \pm 0.10 \times 10^{-5}$	—	—	$1.42 \times 10^{-5} \pm 0.51 \times 10^{-5}$

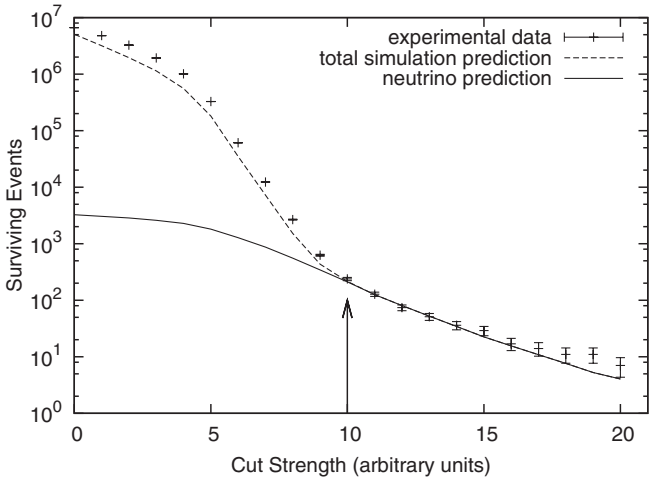

FIG. 1. Data vs cut strength. Shown is the remaining number of events as the cut strength S_{cut} (defined in the text) is varied. Curves are shown for the data and the total simulation prediction. Also shown is the prediction due to atmospheric neutrinos alone. The selection from the text corresponds to a cut strength of $S_{\text{cut}} = 10$, and is denoted by an arrow. At this point, the data are dominated by atmospheric neutrinos.

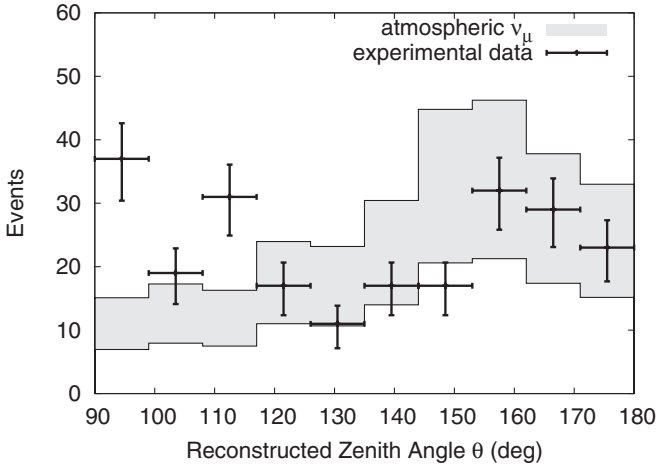

FIG. 2. Distribution of the reconstructed zenith angle θ of the final event sample. A zenith of 90 degrees indicates a horizontal event, and a zenith of 180 degrees is a directly up-going event. The band shown for the atmospheric neutrino simulation includes the systematic errors from the text, and the error bars on the experimental data are statistical. Note that uncertainty due to the atmospheric neutrino flux is an uncertainty in normalization and is nearly independent of a zenith angle.

tween about 10^2 and 10^4 GeV, peaked at 1000 GeV, to survive the analysis cuts.

In 137.4 days of live time we expect $211 \pm 76.1(\text{syst}) \pm 14.5(\text{stat})$ atmospheric neutrino events to survive at $S_{\text{cut}} = 10$ and 234 events are measured. Above a zenith of 120 degrees, where the background contamination is small, we measure 142 events with an expectation of $169 \pm 60.9(\text{syst}) \pm 13.0(\text{stat})$ due to atmospheric neutrinos. The principal systematic uncertainty in this atmospheric neutrino expectation is due to the approximately 30% theoretical uncertainty in the atmospheric flux normalization [7]. The other significant systematic error is due to uncertainties introduced by the modeling of light propagation and the detection efficiency of IceCube DOMs. The uncertainty in the atmospheric neutrino rate due to this modeling is estimated at 20% and is obtained in this initial study by examining changes in the neutrino passing rate when varying the cuts to account for the background simulation disagreement in Fig. 1.

Figure 2 shows the measured zenith distribution for the final event sample along with the atmospheric neutrino prediction. The zenith angle distribution agrees well with atmospheric neutrino simulation for vertical events above about 120 degrees. The observed excess is believed to be residual contamination from down-going single and double cosmic-ray muons. This excess disappears if we tighten the cuts beyond $S_{\text{cut}} = 10$, suggesting that the recorded events at the horizon are of typically lower quality than expected from atmospheric neutrino simulation. This reinforces the belief we are seeing residual background at the horizon. Above about $S_{\text{cut}} = 12$, with low statistics, the data at the horizon are consistent with a pure atmospheric neutrino signal. Figure 3 shows the azimuth distribution with the IC-9 geometry in the inset. The azimuth distribution has two strong peaks corresponding to the long horizontal axis of the IC-9 detector. The cut of 250 meters on event length constrains near-horizontal events that can be accepted along the short axis of IC-9 since the string spacing is 125 meters. We expect more uniform azimuthal acceptance in future seasons as the detector grows and becomes more symmetric.

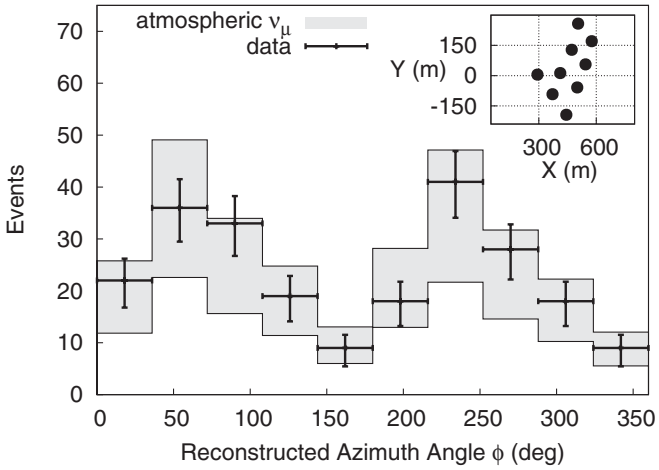

FIG. 3. Distribution of the reconstructed azimuth angle ϕ the final event sample. The band shown for the atmospheric neutrino simulation includes the systematic errors from the text, and the error bars on the experimental data are statistical. The inset shows the horizontal locations of the strings making up IC-9 relative to the center of the future array. Note that uncertainty due to the atmospheric neutrino flux is an uncertainty in normalization and is nearly independent of a zenith angle.

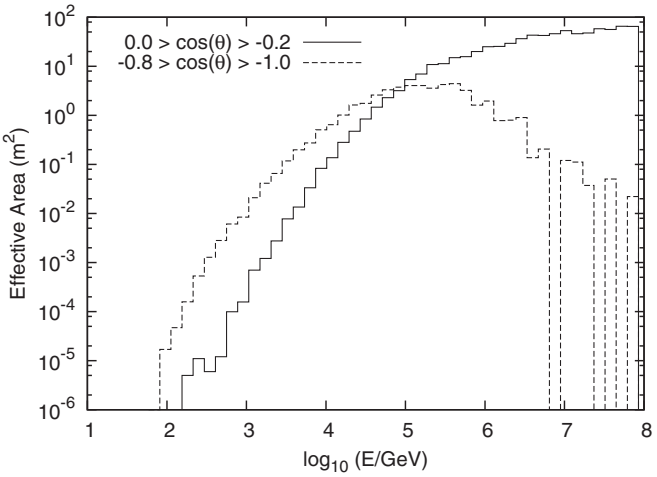

FIG. 4. The effective area of IC-9 to a diffuse source of muon neutrinos. The event selection from the text was used, except that there was no multiplicity requirement imposed on the simulated events. The effective area to muon neutrinos and muon antineutrinos have been averaged to produce the figure. The effective area is shown as a function of neutrino energy, both for vertical and horizontal neutrino events. Horizontal events have a zenith of 90 degrees and vertical up-going events have a zenith of 180 degrees.

We can characterize the response of the detector to neutrinos with an effective area A_{eff} which is a function of neutrino energy E and neutrino zenith angle θ. The function $A_{\text{eff}}(E, \theta)$ is defined as the function which satisfies

$$R = \int dE \int d\Omega \cdot \Phi(E, \theta) \cdot A_{\text{eff}}(E, \theta), \qquad (1)$$

where $\Phi(E, \theta)$ is an arbitrary diffuse neutrino flux and R is the corresponding rate of events surviving analysis cuts. Figure 4 shows the effective area of IC-9 to neutrinos with the event selection of $S_{\text{cut}} = 10$, both for neutrinos near the horizon and for nearly vertical neutrinos. The effective area to neutrinos is much smaller than the geometrical area of the detector, due to the smallness of the neutrino cross section. Above 10^5 GeV, the Earth starts to become opaque to neutrinos, and the highest energy up-going neutrinos can only be detected at the horizon.

IV. CONCLUSIONS

In 2006, IceCube was approximately 10% deployed and acquiring physics-quality data. Atmospheric neutrinos serve as an irreducible background to astrophysical neutrino observation, as a guaranteed source of neutrinos for calibration and verification of the detector, and may be studied as a probe of hadronic interactions at energies inaccessible to terrestrial labs. In the first 137.4 days of live time we have identified 234 neutrino candidates with the IC-9 detector. For events above 120 degrees, this neutrino sample is consistent with expectations for a pure atmospheric neutrino sample. Selection of events was done within six months of the beginning of data acquisition, demonstrating the viability of the full data acquisition chain, from PMT waveform capture at the DOM with nanosecond timing, to event selection at the South Pole and transmission of that selected data via satellite to the north. During the 2006–2007 season, 13 more strings were deployed, bringing the total number of strings for the InIce detector to 22. The deployment of IceCube will continue during austral summers until 2010–2011, while the integrated exposure of IceCube will reach a $\text{km}^3 \cdot \text{year}$ sometime in 2009.

ACKNOWLEDGMENTS

We acknowledge the support from the following agencies: National Science Foundation-Office of Polar Program, National Science Foundation-Physics Division, University of Wisconsin Alumni Research Foundation, Department of Energy, and National Energy Research Scientific Computing Center (supported by the Office of Energy Research of the Department of Energy), the NSF-supported TeraGrid system at the San Diego Supercomputer Center (SDSC), and the National Center for Supercomputing Applications (NCSA); Swedish Research Council, Swedish Polar Research Secretariat, and Knut and Alice Wallenberg Foundation, Sweden; German Ministry for Education and Research, Deutsche Forschungsgemeinschaft (DFG), Germany; Fund for Scientific Research (FNRS-FWO), Flanders Institute to encourage scientific and technological research in industry (IWT), Belgian Federal Office for Scientific, Technical and Cultural affairs (OSTC); the Netherlands Organization for Scientific Research (NWO); M. Ribordy acknowledges the support of the SNF (Switzerland); A. Kappes and J. D. Zornoza acknowledge support by the EU Marie Curie OIF Program.

[1] J. Ahrens *et al.* (IceCube Collaboration), Astropart. Phys. **20**, 507 (2004).
[2] T. K. Gaisser, F. Halzen, and T. Stanev, Phys. Rep. **258**, 173 (1995).
[3] E. Waxman and J. N. Bahcall, Phys. Rev. Lett. **78**, 2292 (1997).
[4] F. W. Stecker, C. Done, M. H. Salamon, and P. Sommers, Phys. Rev. Lett. **66**, 2697 (1991).

[5] A. Achterberg *et al.* (IceCube Collaboration), Astropart. Phys. **26**, 155 (2006).
[6] T. K. Gaisser and M. Honda, Annu. Rev. Nucl. Part. Sci. **52**, 153 (2002).
[7] G. D. Barr, S. Robbins, T. K. Gaisser, and T. Stanev, Phys. Rev. D **74**, 094009 (2006).
[8] K. Münich *et al.* (IceCube Collaboration), in Proceedings of the 29th International Cosmic Ray Conference, 2005 (unpublished).
[9] C. Costa, F. Halzen, and C. Salles, Phys. Rev. D **66**, 113002 (2002).
[10] E. V. Bugaev *et al.*, Phys. Rev. D **58**, 054001 (1998).
[11] A. D. Martin, M. G. Ryskin, and A. M. Stasto, Acta Phys. Pol. B **34**, 3273 (2003).
[12] J. Ahrens *et al.* (AMANDA Collaboration), Nucl. Instrum. Methods Phys. Res., Sect. A **524**, 169 (2004).
[13] D. Heck *et al.*, in Proceedings of the 27th International Cosmic Ray Conference, 2001 (unpublished), p. 233.
[14] G. D. Barr, T. K. Gaisser, P. Lipari, S. Robbins, and T. Stanev, Phys. Rev. D **70**, 023006 (2004).
[15] G. Barr (private communication).
[16] H. L. Lai *et al.* (CTEQ Collaboration), Eur. Phys. J. C **12**, 375 (2000).